Terra Antartica
2000, 7(3), 287-298

Brittle Deformation Patterns of CRP-2/2A, Victoria Land Basin, Antarctica

T.J. WILSON[1*] & T.S. PAULSEN[1, 2]

[1]Byrd Polar Research Center and Dept. of Geological Sciences, The Ohio State University, 1090 Carmack Road, Columbus, OH 43210 - USA
[2]Department of Geology, University of Wisconsin-Oshkosh 800 Algoma Boulevard, Oshkosh, WI 54901 - USA

**Corresponding author* (twilson@mps.ohio-state.edu)

Received 27 October 1999; *accepted in revised form* 7 June 2000

Abstract - Fractures in Quaternary – Lower Oligocene strata cored in the Cape Roberts Project CRP-2A drillhole provide a record of late Cenozoic and contemporary stresses along the Transantarctic Mountains Front structural boundary at Cape Roberts, southern Victoria Land. Natural fractures in CRP-2A core include normal-displacement slickensided faults and closed microfaults, clastic dykes, clastic veins injected along faults, and calcite ± sulfide veins. Microtextures within natural fracture fills document pre-lithification shearing, brittle cataclasis, and mineralization along pre-existing faults during diagenesis. Natural fractures have about the same orientations throughout the Oligocene stratigraphic section, consisting of two dominant conjugate normal fault arrays striking north-northeast and east-west. Natural fracture density increases markedly below unconformities at 307 and 444 metres below sea floor. Drilling- and coring-induced fractures are also abundant in CRP-2A core. The most common induced fracture types are steeply-dipping petal-centreline and core-edge fractures, and subhorizontal disk and other tensile fractures. There is a strong north-northwest preferred orientation to the petal-centreline and core-edge fractures. The natural fracture sets have subperpendicular orientations, suggesting alternation of the least and intermediate principal stresses, due either to regional or local effects. The natural fault and vein sets are parallel to faults mapped onshore in outcrop and offshore from seismic data. Neither the core faults or the regional fault sets are parallel to the Transantarctic Mountains Front rift boundary, suggesting oblique rifting kinematics. In contrast, the north-northwest contemporary maximum horizontal compressive stress is parallel with the Transantarctic Mountains Front, consistent with contemporary east-northeast directed extension across the rift boundary.

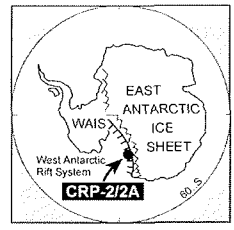

INTRODUCTION

The Cape Roberts Project (CRP) drill holes are situated along the Transantarctic Mountains Front, which is the structural boundary between the uplifted Transantarctic Mountains rift flank to the west and the downfaulted Victoria Land rift basin to the east (Barrett et al., 1995). The Transantarctic Mountains Front is considered here to encompass both onshore and offshore faulting accommodating the large-scale differential relief across this boundary. The CRP sites were selected with the goal of sampling the east-dipping strata of the Victoria Land basin that climb to the sea floor along this margin. The sedimentary strata of the Victoria Land basin have been imaged seismically throughout much of the Ross Sea, yet the ages of many of the seismic reflectors remain uncertain because they have not been sampled by drilling and dated. The CRP-1 and CRP-2/2A drill holes penetrated an aggregate thickness of *c.* 600 m of mainly Miocene - Oligocene sedimentary strata with minor interbedded volcanics, of substantially younger age than predicted based on regional seismic correlations (Cape Roberts Science Team, 1998, 1999). No rock units spanning the same time interval crop out in the region, although late Cenozoic volcanic rocks are widespread ~100 km south-southeast of the drilling locality.

The CRP drill sites are situated on the western margin of an offshore bathymetric high known as Roberts Ridge (Barrett et al., 1995). CRP-2/2A was drilled on the western slope of Roberts Ridge in 180 m of water and penetrated 624 m beneath the seafloor. The slope of Roberts Ridge trends in a north-northeast (N10E) direction, with the downslope gradient west-northwestward into a local topographic trough between the ridge and the shoreline.

Documentation of brittle fracture patterns in the core and in the borehole walls is aimed at understanding the stress and strain history of the Transantarctic Mountain Front structural boundary. Because Cretaceous-Neogene age rocks do not crop out in the Transantarctic Mountains in south Victoria Land, except for local Neogene volcanic rocks, it has been difficult to precisely constrain the timing of rift-related structures found in mountain outcrops (*e.g.*, Fitzgerald, 1992; Wilson, 1992, 1995). Structural analysis of offshore seismic reflection profiles in the western Ross Sea has documented discrete episodes of faulting associated with development of the Victoria Land Basin and its younger axial portion, known as the Terror rift (Cooper et al., 1987; Del Ben et al., 1993; Salvini et al., 1997). Salvini et al. (1997) differentiated Cenozoic faulting episodes in the western Ross Sea using a regionally developed unconformity surface as a marker. The seismically-mapped unconformity was taken to be ~30 Ma, based on age data from the eastern Ross Sea (Busetti, 1994), but the age of this boundary was poorly constrained in the western Ross Sea. Salvini et al. (1997) interpreted a ~55-30 Ma episode of extension associated with Transantarctic Mountains

uplift and a post-30 Ma transtensional episode associated with dextral strike-slip faulting across northern Victoria Land. Mapping brittle deformation patterns in Victoria Land basin strata cored during CRP drilling can provide important new age control for Cenozoic deformation along the Transantarctic Mountain Front. Moos et al. (this volume) report on fractures mapped from borehole televiewer (BHTV) imagery in the CRP-2A borehole wall. In this paper we focus on fractures logged in CRP-2A core.

METHODS

The CRP utilizes a wireline diamond drilling system deployed on a floating platform of annual sea ice that is ~ 2m thick; during the period of drilling operations the sea ice is fixed to the shore and has minimal relative motion with respect to the coast (Cape Roberts Science Team, 1998. 1999). The downhole dipmeter log established that the CRP-2A borehole is within 1 degree of vertical (Cape Roberts Science Team, 1999; see Jarrard et al., this volume). The triple-tube coring system yielded 95% core recovery. In CRP-2, the drilling operation reached 57.5 metres below sea floor (mbsf). Following withdrawal and reentry of the drill stem, drilling created a new drill hole that partly recovered a stratigraphic interval that overlaps with core from CRP-2. This second drill hole and core is called CRP-2A and is the focus of this paper. The CRP-2A drilling operation recovered approximately 200 m of 61 mm diameter core (HQ) and 424 m of 45 mm diameter core (NQ). Once the core was recovered and depths were assigned to the top and bottom of the core run, we logged each fracture in the whole core at the CRP drill site laboratory. Depths to fracture top and bottom were recorded to the nearest centimetre; here we have rounded depths to the nearest metre. The dip and dip direction of each fracture was measured with respect to an arbitrary 'north' defined by a red line scribed the length of each core run. We also systematically recorded any bedding offsets, crosscutting or abutting relations between fractures, type of fracture fill, and presence of surface fractographic features.

After the fracture logging, we used the DMT CoreScan® instrument to scan segments of the whole core that were up to 1 m long if the integrity of the core permitted handling. The whole-core scans were then digitally stitched together into longer intervals using software provided by DMT. We stitched together sections of core where no internal relative rotation of the core occurred during drilling and coring (*i.e.*, intact core intervals). The intact core intervals were reorientated to *in situ* coordinates using procedures presented in Paulsen et al. (this volume); these primarily relied on matching fractures between core and orientated BHTV imagery. At present, approximately 39% of CRP-2A core has been orientated (see Tabs. 1 & 2 in Paulsen et al., this volume). Fracture strikes discussed here refer only to those fractures that occur within orientated core. Our data set from the orientated core comprises 63 faults, 103 veins and 64 petal-centreline and core-edge fractures. Dip directions on our plots are likely biased toward easterly dips due to a $\pm 180°$ ambiguity in strike azimuth for portions of the orientated core intervals (Paulsen et al., this volume).

Thin sections of 27 samples of CRP-2A core were examined in order to characterize the microscopic textures of core fractures that were closed and therefore did not permit examination of surface fractographic features. We conducted this work to search for microscopic kinematic indicators and to analyse microtextures that would establish whether the fractures represent clastic intrusions, veins or fault zones, as inferred from macroscopic logging.

FRACTURES IN CRP-2A CORE

NATURAL FRACTURES

Pre-existing fractures that are intersected during coring are termed 'natural' fractures. Natural fractures must be distinguished from drilling- and coring-induced fractures in order to correctly interpret fracture mode of origin and thus to reconstruct strain and stress patterns from them. Here we describe a variety of natural fractures from CRP-2A core and interpret their mode of origin based on macroscopic form, surface features, relation to bedding, dip angle, and microstructures. We make a case for a tectonic origin for these structures, but acknowledge that it is not always possible to reliably distinguish between tectonic fractures and pre-lithification structures formed by non-tectonic processes, such as mass wasting and subglacial shearing (see Passchier, this volume).

Faults

Open Faults. Discrete open fractures with highly polished, slickensided and striated surfaces were present between 189 and 525 mbsf, though most occurred above 330 mbsf in CRP-2A core (Fig. 1). Slickensided fault surfaces are common in lithified rock, where it is generally considered that abrasion during frictional sliding polishes and grooves the fault surface (*e.g.* Suppe, 1985). Polished and striated surfaces have also been reported in deformed but unlithified argillaceous sediments (*e.g.*, Maltman, 1987). In CRP-2A core, slickensided faults were found in mudstone, siltstone and fine-medium sandstone. In one case, a highly polished surface occurred in poorly lithified sandstone, where the fault had a 1-2 cm margin of cemented material, suggesting that this material was previously more well-lithified, but lost cement through diagenetic processes. The fact that the slickensided faults do not occur solely in clay-rich sedimentary rock suggests that they formed in lithified material due to frictional processes. All of the open faults had surface fractographic features indicating normal-sense shear, however the lack of displaced markers precluded constraining displacement magnitudes.

Closed Faults. Some faults occurred as closed fractures across which bedding planes are offset (Fig. 2). With a few, rare exceptions, all of these are microfaults with normal-sense dip-separation of bedding of 2-12 mm.

Fig. 1 - Polished and striated slickensided brittle fault surface. Core is 61 mm in diameter.

Fig. 2 - Set of 3 normal-sense displacement microfaults in Lower Oligocene strata. Unrolled image of surface of 45-mm diameter whole core. Note the discrete mm-thick fault zones sharply truncate the pre-lithification folds. Arrows denote apparent sense of motion. Discrepancies in magnitude of apparent offset of layers across the fault are attributed to displacement of layers with variable dips and thicknesses due to the soft-sediment folding.

Because these microfaults were sealed, it was not possible to examine the fault surfaces for striae. There is evidence that some microfaults formed by pre-lithification deformation associated with point loading by lonestones (R. Powell, pers. comm.), or possibly formed during mass movement and/or glacial shearing (Passchier, this volume). Structures we logged as closed microfaults were discrete planes or narrow, planar, mm-scale bands that crossed the entire core and that always cross-cut any folding, convolute bedding and other structures formed by pre-lithification deformation of the strata (Fig. 2). We acknowledge, however, that based on meso- or microstructure alone, it is difficult to discriminate between synsedimentary or glaciotectonic microfaults and those microfaults that formed by tectonically-induced shearing.

We collected a suite of samples to attempt to identify microstructures diagnostic of either pre-lithification shearing, where high water content would promote ductile behaviour, or of brittle deformation of dewatered or lithified material. One microfault cutting siltstone to fine sandstone, consisted of a few mm-thick dark-colored zone with normal-sense offset of bedding (Fig. 3a). This dark zone parted to reveal polished and striated slickenside surfaces within it. Microscopic examination showed that this microfault zone has reduced grain-size, angular grains of a range of size from sand to clay, and a 'braided' or anastomosing internal fabric, all contained within a planar zone with margins that sharply truncate bedding (Fig. 3b). Anastomosing fabrics can form during shearing of water-rich ductile sediment (*e.g.*, Maltman, 1987, 1988) and comminution of grains can take place in unlithified sediment undergoing high shear strains (*e.g.* Iverson et al., 1996). However in these low-strain shear zones, the sharp boundaries and marked grain-size reduction appear most consistent with cataclasis during brittle shear of dewatered or lithified material. Most of the microfaults examined microscopically have textures compatible with this type of brittle deformation. In a few cases we observed some flexural drag of bedding adjacent to the microfault planes, but more commonly bedding is truncated sharply and displaced (Fig. 3b). The grain size reduction in the microfault zones is indicative of brittle cataclasis. The microfault zones characteristically have a pronounced preferred orientation of clast long axes parallel to the fault zone. The grain shape fabric and anastomosing pattern of the fault strands are typical of brittle fault-zone textures, although these textures do not rule out origin by pre-lithification shearing. Indeed, microscopic examination showed that some microfaults consist of probable pre-lithification 'shear zones', where substantial drag of bedding occurs across diffuse zones with no associated grain-size reduction, and therefore indicate shear without brittle cataclasis. Brittle microfaults are distinguished from clastic injections along faults by having smaller and more uniform grain size than the host rocks.

Microscopic examination of structures originally described macroscopically as veins at the drill site and sedimentology labs, mainly prove to be microfaults overgrown or replaced by calcite ± sulfides. In the depth range of 509-520 mbsf, grey carbonate cement is preferentially developed along discrete fault planes. At depths of 440 mbsf and greater, microfaults typically appear macroscopically to be very thin (0.5-2 mm) white to pale grey veins. These 'veins' , which locally have conjugate geometry and mutual offset relations, are particularly abundant between 535-544, 555-558, and 564-566 mbsf. All of these 'veins' examined in thin

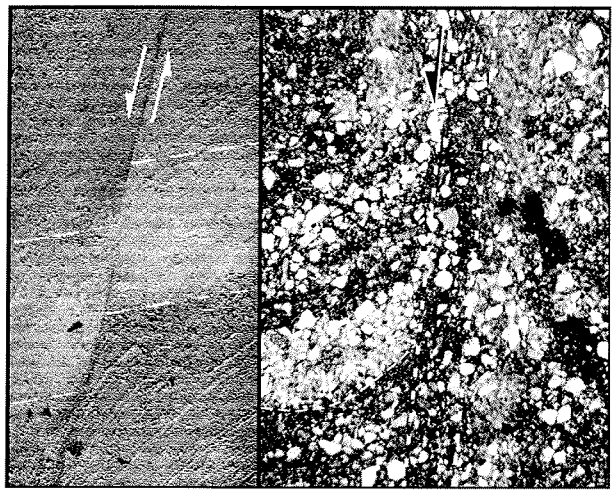

Fig. 3 - A. Normal-sense microfault truncates and offsets bedding (white dashed lines). Note dark zone along microfault. Slabbed core is 45 mm diameter. B. Thin section of microfault. Note fault zone (bounded by short white dashed lines) with reduced grain size and anastomosing zones of clay-size material. Fault zone sharply truncates bedding (long white dash lines), which shows slight flexural drag.

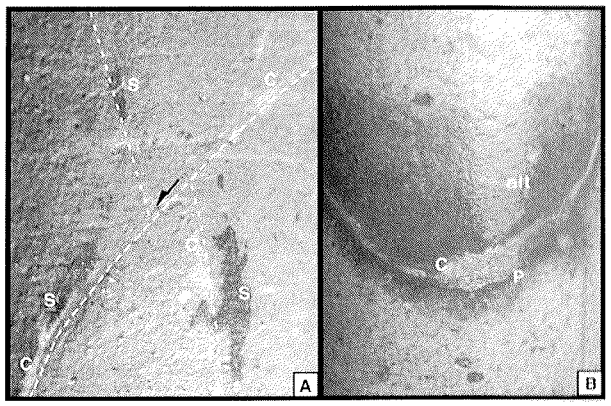

Fig. 4 - A. Hairline veins defined by white calcite (C) and dark sulfide patches (S). Note conjugate geometry and normal-sense offset of one fault by another. Thin section examination showed that calcite and sulfides were precipitated along pre-existing microfaults. B. Wider vein with pyrite (P) interlayered with calcite (C) with dark alteration bands (alt) along vein margins. Photos of whole core, 45 mm in diameter.

section are either thin clastic injections along fault planes or, more commonly, mineral growth along pre-existing fault planes. The latter have patchy development of calcite overgrowing the fault zone fabrics described above, indicating precipitation along a pre-existing microfault. These relations suggest that most microfaulting occurred prior to this episode of mineralization.

Veins

Clastic Intrusions. Gray, white, and brown, planar bands 2-15 mm wide that crosscut bedding commonly occur in the CRP-2A core (Cape Roberts Science Team, 1999). Some thicker, coarse-grained end members could be distinguished as clastic dykes during initial core description (Cape Roberts Science Team, 1999). Many thin, very fine-grained pale bands were classified macroscopically as either sediment-filled fractures or veins (Cape Roberts Science Team, 1999). In our thin section examination, some of the thin 'veins' proved to be sediment fill. These are most reliably distinguished where the grain size in the vein is coarser than the adjacent host rock. Sedimentary injection is also indicated where the vein fill is clastic and of uniform grain size that differs from that of the adjacent wall rock. The clastic dykes and thin, sedimentary injections commonly have calcite in the matrix and contain disseminated or localized pyrite. Some of these pale veins proved to be microfaults associated with calcite replacement. We have not yet identified reliable macroscopic criteria to systematically discriminate fine-grained sediment-filled fractures from mineralized veins. In this paper, therefore, we have grouped these fractures together as 'veins' in the distribution and orientation analyses that follow.

Clastic dykes commonly form as opening-mode hydraulic fractures which, at least near the surface of the earth, tend to have a subvertical dip. The clastic dykes and thin, sediment-filled fractures that we have identified in CRP-2A core have dips between 50-80°, with most ranging from 60-75°. Such dips are more typical of shear fractures than of subvertical tensile fractures (*e.g.* Engelder, 1987). In several cases, the thin clastic veins followed microfaults, *i.e.* there was normal-sense offset of bedding across the sediment-filled fracture plane. This relationship clearly shows that some microfaults formed prior to complete lithification of the strata. In one case sediment-filled microfaults occur in conjugate arrays, with equal and opposite dips and mutual crosscutting relations. The development of conjugate fracture arrays over several metres of strata (*e.g.*, 523-528 mbsf) suggest a larger-scale stress control rather than local vertical loading, such as the emplacement of lonestones.

Calcite ± Sulfide Veins. A large number of fractures in CRP-2A core below 400 mbsf were described macroscopically as calcite veins. Such veins range from barely perceptible 'hairline' veins ≤1 mm in width, up to 15-20 mm wide (Fig. 4). Patches or discontinuous and irregular layers of sulfides are commonly associated with the veins and some show a pervasive green alteration of the adjacent host rock for up to 30 mm from the vein margins (Fig. 4).

Thin section examination of a subset of these veins shows that most represent normal-sense microfaults that have been mineralized by calcite. The carbonate mineralization typically has not completely replaced the original microfault shear fabric, and instead has overgrown or replaced it in patches. Disseminated and patchy sulfide mineralization also preferentially occurs along the microfaults. These types of 'veins' commonly occur in conjugate arrays with mutual offsets between oppositely dipping veins (Fig. 4a). The microscopic textures along these conjugate arrays show that microfaulting developed prior to mineralization.

A few wider veins that consist of interlayered sulfide and calcite are not associated with bedding offset. Sulfides commonly dominate the veins and the calcite typically occurs as discrete internal layers, suggesting the calcite

may have formed along a later fracture. There are no textures in the veins that indicate either shear- or opening-mode displacement across the fracture.

A small proportion of the veins observed between 565-608 mbsf have macroscopic and microscopic morphologies that are characteristic of tensile, opening-mode veins formed by the 'crack-seal' mechanism, in which repeated opening and vein precipitation occurs (Ramsay, 1980). These include macroscopic compound veins composed of multiple strands, which microscopically are characterized by clasts cut by multiple veins and fibrous calcite overgrowths with fibers orientated perpendicular to vein walls. Rare veins with en echelon, overlapping segments are also likely of tensile origin. Veins with this mode of origin have dips between 20 and 83°. The shallow dips are atypical of tensile fractures.

Orientations of Faults and Veins

Faults and veins have been plotted in discrete depth intervals representing different ages and major unconformity-bounded stratigraphic packages in the CRP-2A core (Fig. 5). We do not currently have orientated fracture data from Quaternary or Pliocene strata and have only very sparse orientated data for fractures in Lower Miocene and Upper Oligocene strata. The fault and vein data sets only have significant populations for the Lower Oligocene section. The orientated data represent only ~62% of faults and veins logged. The classification of fractures as either faults or veins during our macroscopic core logging is nonunique in that our subsequent microscopic analysis has shown that many, if not most, of the 'veins' follow normal fault planes. We maintain our original fracture classifications for this analysis, but note the cases where discrimination based on microtextures allows additional correlations to be made.

The first stratigraphic interval includes Lower Miocene and Upper Oligocene strata down to an unconformity at 307 mbsf, tentatively assigned as the Upper/Lower Oligocene boundary (Wilson et al., this volume). If the few available data from this interval are representative, there appears to be a north-northeast-striking conjugate normal fault set, a similarly orientated NE-striking vein, and one NW-striking fault cutting Miocene strata. These faults and veins are likely younger than ~20-21 Ma, the age of the youngest strata cut by the fractures.

The next stratigraphic interval is an unconformity-bounded package of Early Oligocene age extending from 307-444 mbsf. The fault sets in these Lower Oligocene strata have average orientations of N70W, 64 NE and N34E, 49SE. Though poorly defined in the available fault data, there are a few NE-SW-striking, NW-dipping planes that may form a conjugate set with the latter. Veins in these Lower Oligocene strata have a dominant average attitude of N25E, 32SE. There are a few NE-SW-striking, NW-dipping veins that may define a conjugate pair. Based on the core observations of conjugate geometry of the faults and veins, and the bias toward eastward dips because of the core orientation methods, it is likely that the conjugate patterns of faults and veins are real. The veins in this interval have a relatively low-angle eastward dip, atypical of either tensile fractures or of conjugate normal faults. Veins plotted for this depth interval consist of many sediment-filled fractures, indicating that they formed before complete lithification of the sequence. The low dips may, therefore, be the result of early-formed, steep fractures that have been rotated to a shallower dip as the sediment compacted. It is interesting, however, that the strike directions of faults and veins are similar, suggesting that the same stress regime controlled both the inferred early, pre-lithification fractures and the later brittle faults that cut the sequence. All of the faults and veins in this interval may be younger than 24 Ma, the youngest strata in this interval. Alternatively, if the interpretation of pre-lithification fracturing is correct, than the age of at least some of this deformation would be close to the age of the strata, or up to ~27 Ma.

The lower part of the core, consisting of Lower Oligocene strata extending from the unconformity at 444 mbsf to the base of the cored interval at 625 mbsf, has a larger natural fracture population. It is this depth range for which the fault and vein populations are likely to overlap, in that many of the veins are replacing microfaults. Faults in this depth range have a dominant strike of N78W, with a 58° dip to the north. A conjugate set has the same strike and dips to the south. A subordinate fault set strikes northeast (N18E), with an average dip of 61° east. Veins show a similar, but not identical, pattern. The two dominant vein populations have average orientations of N86E, 69° N and N4W, 69° W. There appear to be conjugate pairs to both of these vein sets. In this portion of the core, conjugate geometries were commonly observed for both faults and veins (*e.g.*, Fig. 4a). These relations indicate that the faults and veins both represent conjugate shear fracture arrays. The faults and veins in this interval must be younger than ~30 Ma, the age of the youngest strata in this interval.

Figure 6 shows the orientations of those veins that are definitely tensile in origin, based on macroscopic geometry and/or microtextures. These tensile veins have a consistent east-northeast strike. The moderate dip angles of many of the veins and the apparent conjugate dip directions are more typical of shear fracture sets than of tensile fractures (*e.g.*, Engelder, 1987).

We consider that the difference in fault and vein orientations is within the error of our reorientation methods, and therefore that faults and veins maintain approximately the same orientation in each of the age-defined sequences. The dominant patterns are north-northeast- and east-west-striking conjugate normal fault arrays (Fig. 5D). Both north-northeast and east-west striking faults occur throughout the Lower Oligocene strata and may also characterize the Lower Miocene–Upper Oligocene section, but data in the younger rocks are still too sparse to draw conclusions regarding orientation patterns of faults in the different age intervals. We have not observed a systematic change in dip angle of fracture sets downcore, even though seismic profiles (Henrys et al., this volume) and dipmeter log analysis (Jarrard et al., this volume) indicate that bedding dips increase from 2-3°s at the top of the section to up to 15° near the base.

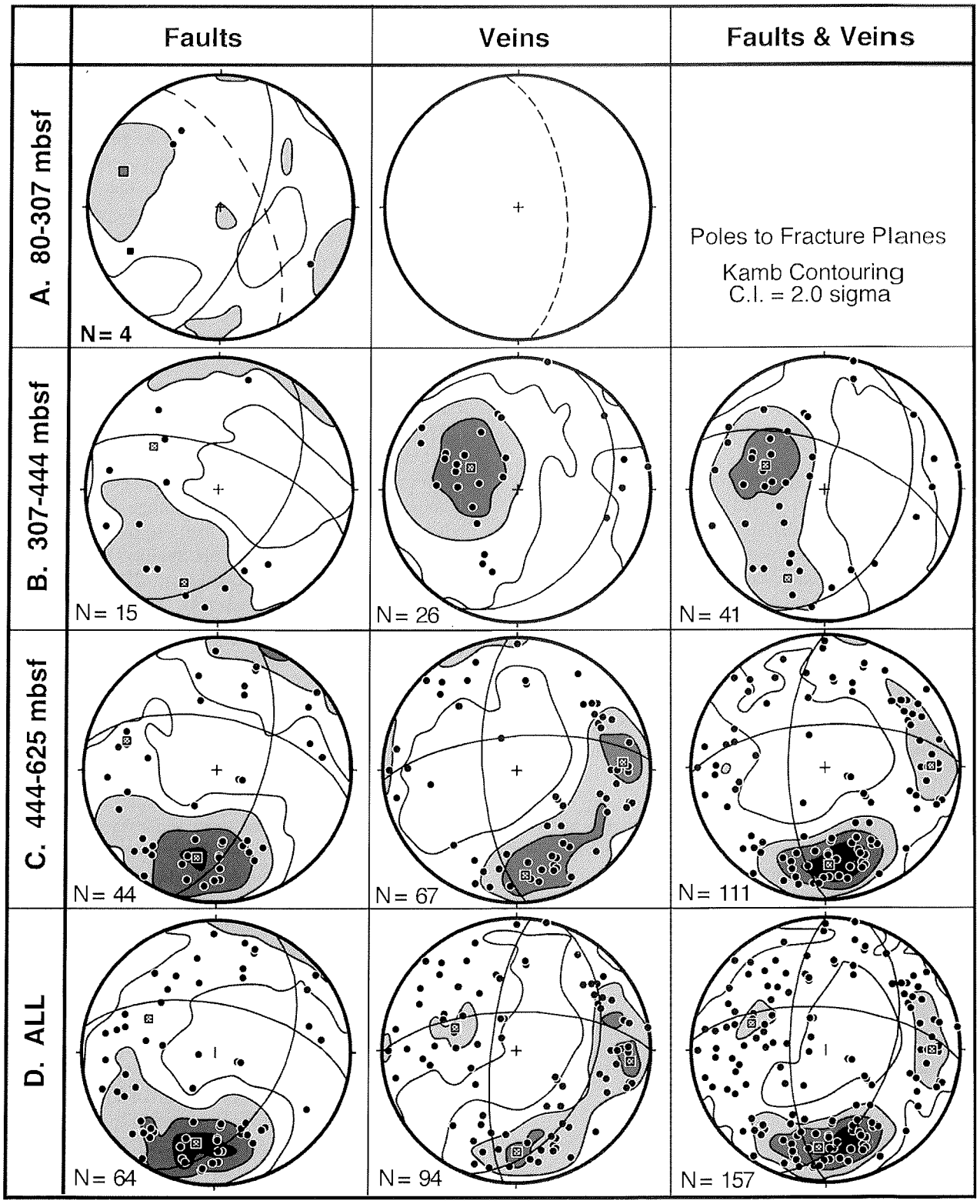

Fig. 5 - Stereoplots of fault and vein attitudes from orientated core. A: Faults and veins in Lower Miocene (dashed lines) and Upper Oligocene strata between 80-307 mbsf; B: Faults and veins from Lower Oligocene section between 307-444 mbsf. C: Faults and veins from Lower Oligocene section between 444-625 mbsf. D: Cumulative plots of faults and veins in Lower Miocene to Lower Oligocene strata in orientated CRP-2A core. Equal-area, lower-hemisphere plots. Great circle curves denote average orientation of fault and vein sets.

FRACTURES OF INDETERMINATE ORIGIN

A significant proportion of the CRP-2A fracture population lacked surface fractographic features, hence we were unable to directly determine the fracture mode of origin. These fractures occur throughout the core. The dip angles of these fractures are shown in figure 7, excluding subhorizontal fractures (classed as dips $\leq 25°$), which likely represent induced tensile fractures. The dip plot shows a bimodal distribution, with peaks at 36° and 66°. The overall average dip of these fractures is 51°. The average dip of both faults and veins is 63° (Fig. 7),

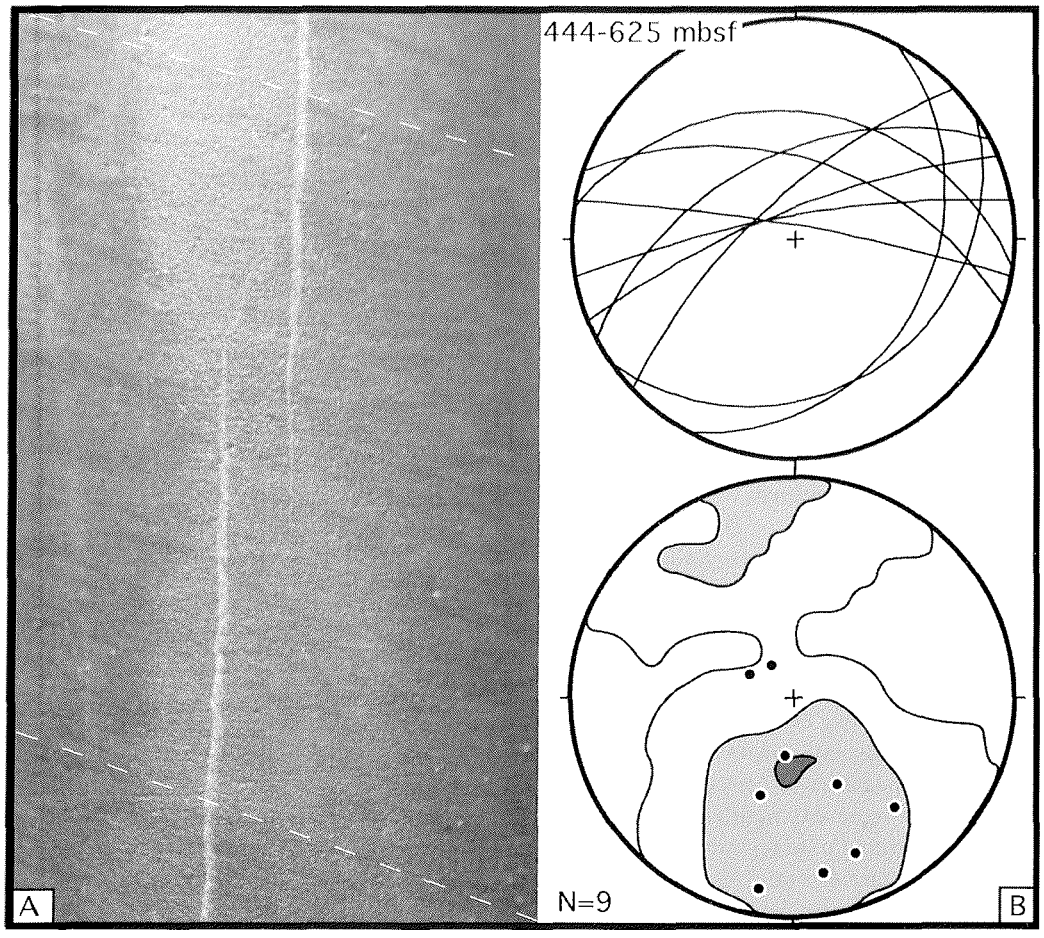

Fig. 6 - A. Example of subvertical calcite vein showing en echelon, overlapping segments with curving tip, typical of tensile, opening-mode fractures. B. Great circle plot (upper) and Kamb contour plot (contour interval = 2 sigma) of poles to tensile veins in Lower Oligocene strata.

comparable to the steeper peak in the undefined fracture population. Steeper fractures in the indeterminate fracture population commonly had small offsets of the core margin along the fracture plane, indicating that motion along the fracture occurred during entry of the core into the core barrel. This, and the 60° dip identical to the natural faults and veins, suggest that the steep subset of the population are natural shear fractures that lacked diagnostic surface slickensides or striae. We have no means to determine the fracture mode for the remainder of the population, although future work comparing the strike and dip patterns of these fractures to faults and veins may allow interpretation of likely fracture origins.

INDUCED FRACTURES

Stresses imposed on the host rock and on the core due to drilling and coring operations can cause fractures to form around the borehole and within the core. Numerous empirical and analytical studies have demonstrated that

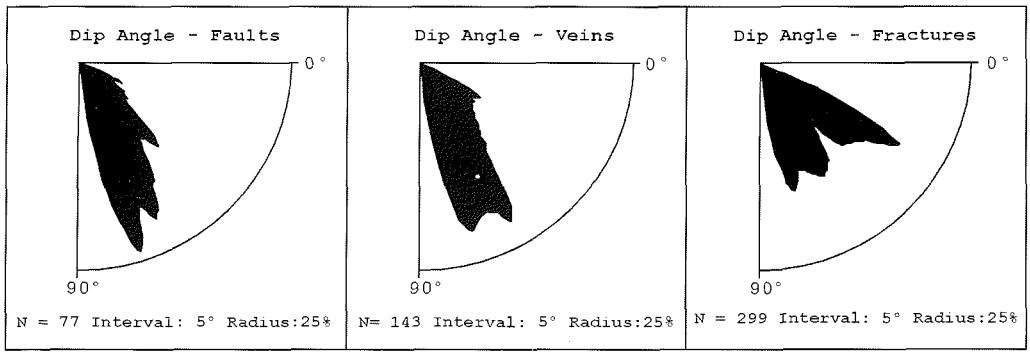

Fig. 7 - Smoothed rose diagram plots of dip angles of faults, veins, and fractures of indeterminate origin in CRP-2A strata. Faults and veins have average dips of 63°, consistent with their formation as shear fractures. The fractures have a bimodal distribution with peaks at c. 60 and 35° dips.

these "induced" fractures propagate in trajectories that are primarily controlled by the modern stress field acting on the crust (Kulander et al., 1990; Lorenz et al., 1990; Bankwitz and Bankwitz, 1995; Li and Schmitt, 1997, 1998). The unique shapes and surface fractographic features reflecting the fracture propagation trajectories allow induced fractures to be discriminated from natural fractures; the fracture strikes and/or propagation directions can in turn be used to determine the orientation of the *in situ* horizontal stresses in the vicinity of the borehole. A variety of induced fractures were very common in the CRP2-2A core. Moos et al. (this volume) discuss fractures in the borehole walls that are interpreted to be induced by drilling.

Petal and Petal-Centreline Fractures

Petal fractures have curved shapes, becoming steeper in the downcore direction. They are typically modeled as tensile fractures following stress trajectories that radiate beneath the advancing drill bit (Lorenz et al., 1990; Li and Schmitt, 1997, 1998). Petal fractures may terminate within the core or may propagate along the core axis as vertical "centreline" fractures that die out downwards within the core. The downcore propagation of centreline fractures has been interpreted to represent hydraulic fracturing under the influence of drilling mud pressures (Lorenz et al., 1990). The abundant petal and petal-centreline fractures within CRP2-2A core are characterized by the typical concave-downcore shape and commonly have surface fractographic features that indicate a tensile origin and downcore fracture propagation (Fig. 8A).

Core-edge Fractures

Core-edge fractures in CRP-2A are subvertical, scoop-shaped 'flakes' that occur along the edge of the core (Fig. 8B). Hackle plumes and arrest lines on the core-edge fracture surfaces document tensile fracture mode and down-core fracture propagation. Core-edge fractures were common at the top of core runs, suggesting that they were induced when the drill string tagged the bottom of the hole prior to recommencing coring. It was also common for core-edge fractures to occur on only one side of the core. We interpret the core-edge fractures to be a morphologic variant of petal-centreline fractures, where coring intersected the steep sector of fractures whose trajectories parallel the borehole margin.

Orientation of Petal, Petal-Centreline, and Core-edge Fractures

The strike directions of petal, petal-centreline and core-edge fractures within intervals of CRP-2A core that could be orientated by matching them with the strike of induced, tensile borehole wall fractures mapped in orientated BHTV imagery are shown in figure 9. There is a strong preferred orientation of fracture strike in the north-northwest - south-southeast direction. Empirical and modeling studies have demonstrated that the strikes of the these fractures parallel the maximum horizontal *in situ*

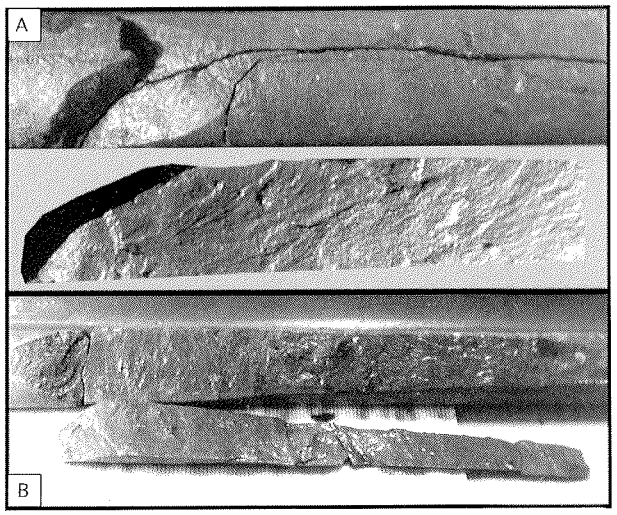

Fig. 8 - A. Petal-centreline fracture in CRP-2A core. Note distinctive curved shape (upper) where petal segment curves inward from core margin to become subvertical centreline fracture in the downcore direction. The fracture surface (lower) shows an arrest line and plumose structure documenting downcore fracture propagation and a fracture origin point just outside of the core margin. B. Core-edge fracture in CRP-2A core. Note scoop-shaped flake, curving in from core margin, propagating down core, and shallow exit angle. Up core to left in all photos.

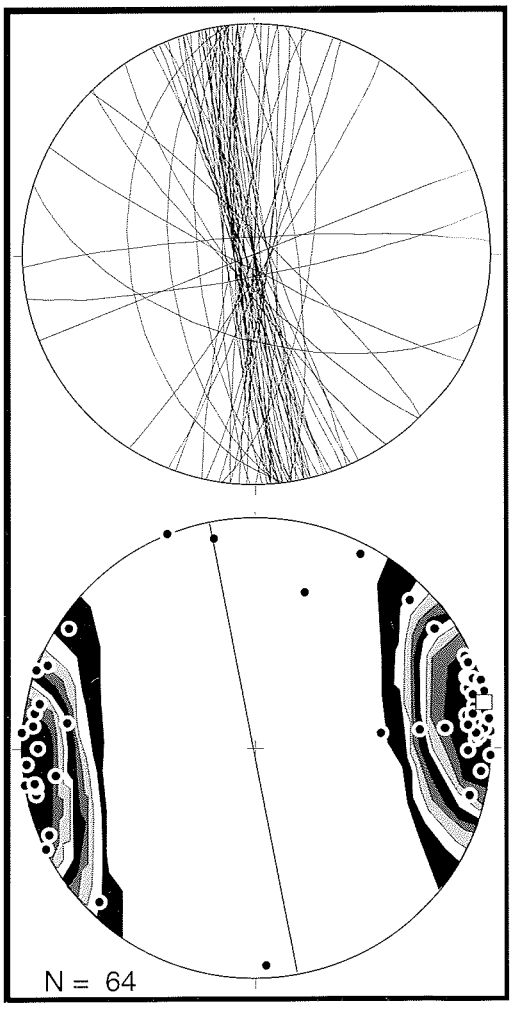

Fig. 9 - Great circle plot and Kamb contour plot (contour interval = 2 sigma) of poles to petal-centreline and core-edge fractures in orientated portions of CRP-2A core. Note very strong preferred orientation with an average strike of N10W.

stress direction in the crust (Plumb & Cox, 1987; Li and Schmitt, 1998). It is important to note that the average N10W strike of petal-centreline and related fractures is oblique to the N10E trend of the bathymetric slope where the drillhole is sited. We suggest, therefore, that the induced fractures record the orientations of regional crustal stress, rather than the local topographically-induced stresses along the flank of Roberts Ridge.

Disc Fractures

Disc fractures are subhorizontal, planar to curviplanar tensile fractures formed due to axial tension as the core is released from the host rock (Kulander et al., 1990; Li and Schmitt, 1998). Subhorizontal fractures are abundant in CRP-2A core. In lithified and cemented core intervals, subhorizontal fractures commonly show fractographic features that include origin points, hackle plumes, and twist hackle at core margins, all indicative of a tensile origin and pointing to nucleation of the fracture within the core. These characteristics allow these fractures to be confidently ascribed to an induced, rather than a natural, fracture origin. Several of these had a distinct, concave-upward 'saddle' shape, which is a typical geometry of induced disc fractures (Bell, 1996; Bankwitz and Bankwitz, 1995). Regular spacing, which is another typical attribute of disc fractures (*e.g.*, Obert and Stephenson, 1965), is not seen in the CRP-2A core however. Here we tentatively interpret subhorizontal fractures of tensile origin as disc fractures, but recognize that some may form by other coring-induced mechanisms, discussed below. In some core runs we found multiple disc fractures with a systematic orientation of hackle plume axes, suggesting control on fracture propagation by the *in situ* stress field. However we have not yet accumulated enough data from orientated core intervals to test whether there is a uniform geographic trend to the plume axes.

Other Drilling- and Coring-induced Fractures

In cases where the cored strata were strongly indurated, mainly in the lower interval of CRP-2A core, induced fractures with well-developed tensile fractographic features developed at the breaks between core runs and coincident with the core catcher tool at the base of the run. Some of the subhorizontal tensile fractures within the core may have formed when the hydraulic drilling apparatus raised the chuck at the top of the drill string, which occurred every 60 cm within a coring run.

Fractures formed from rotation and coring-induced torsion of the core were abundant in CRP-2A core. Spin-off fractures are subhorizontal breaks formed when the drill string lifted and broke the core at the bottom of the hole, allowing rotation of the core as the drill bit re-engaged the bottom of the drill hole. These fractures are distinguished by circular grooves that document relative rotation of core segments. Torsion fractures form due to twisting motion of the core when the rotating drill string applies torque to the core barrel. These curving, tensile fractures were particularly common in poorly indurated, clay-rich intervals and near the bottom of core runs where advance of the core into the core barrel was slower and more difficult.

Handling of the core also induced core fractures, which were predominantly subhorizontal.

DISTRIBUTION OF FRACTURES

Fracture Densities in CRP-2A Core

Fracture densities, counted as number of fractures per metre of core, are displayed in histograms smoothed by a 10-metre moving average window (Fig. 10). For comparison purposes we show in equivalent depth plots the age boundaries, the lithostratigraphic column, and sequence boundaries identified in CRP2-2A core, followed by plots of fracture densities vs. depth. Major age boundaries, marked by unconformities are highlighted and coincide with the depth divisions used for the fracture orientation plots.

Natural fractures are represented by plots of normal faults and veins vs. depth. It should be noted however, that these categories overlap in that the sediment-filled and mineralized veins commonly follow normal faults. Normal faults and veins first show up in significant quantities below 300 mbsf. Within the lower, unconformity-bounded Lower Oligocene section, a major peak in fault density occurs at 320 mbsf, with peaks in vein density slightly deeper at 340 and 370 mbsf. A large population of these veins represents sediment-filled fractures and clastic dykes. Within the Lower Oligocene section below 444 mbsf, both faults and veins have an overall high density. The largest fault density peak is at 530 mbsf, with three major peaks in vein density at 550, 570, and 610 mbsf.

A plot of petal, petal-centreline, and core-edge fractures vs. depth represents induced fracture density. In contrast to the natural fracture density plots, the induced fractures are distributed throughout the entire core. Overall, induced fracture density decreases with depth. Members of the drill crew reported that drilling rate was impeded and the loss of drilling mud increased at many of the depths where these fractures were abundant. Drilling conditions were generally more uniform and the progression of drilling was smoother in the more indurated, lower portion of the cored interval.

Correlation of Fracture Densities and Other Core Attributes

No systematic association of natural fractures with a particular lithology or grain size is evident from the plots, except the low numbers of fractures in loosely consolidated sand horizons. It is possible that shears formed in the sand intervals, but were not macroscopically visible due to minimal grain size reduction or were not preserved due to disturbance of the sediment. In contrast, most peaks in abundance of the petal-centreline fracture group coincide with fine-grained lithologies. In these clay-rich sections, entry of the core into the core barrel was more difficult, resulting in changes in penetration rate. Presumably this was also associated with changes in weight on the bit and/

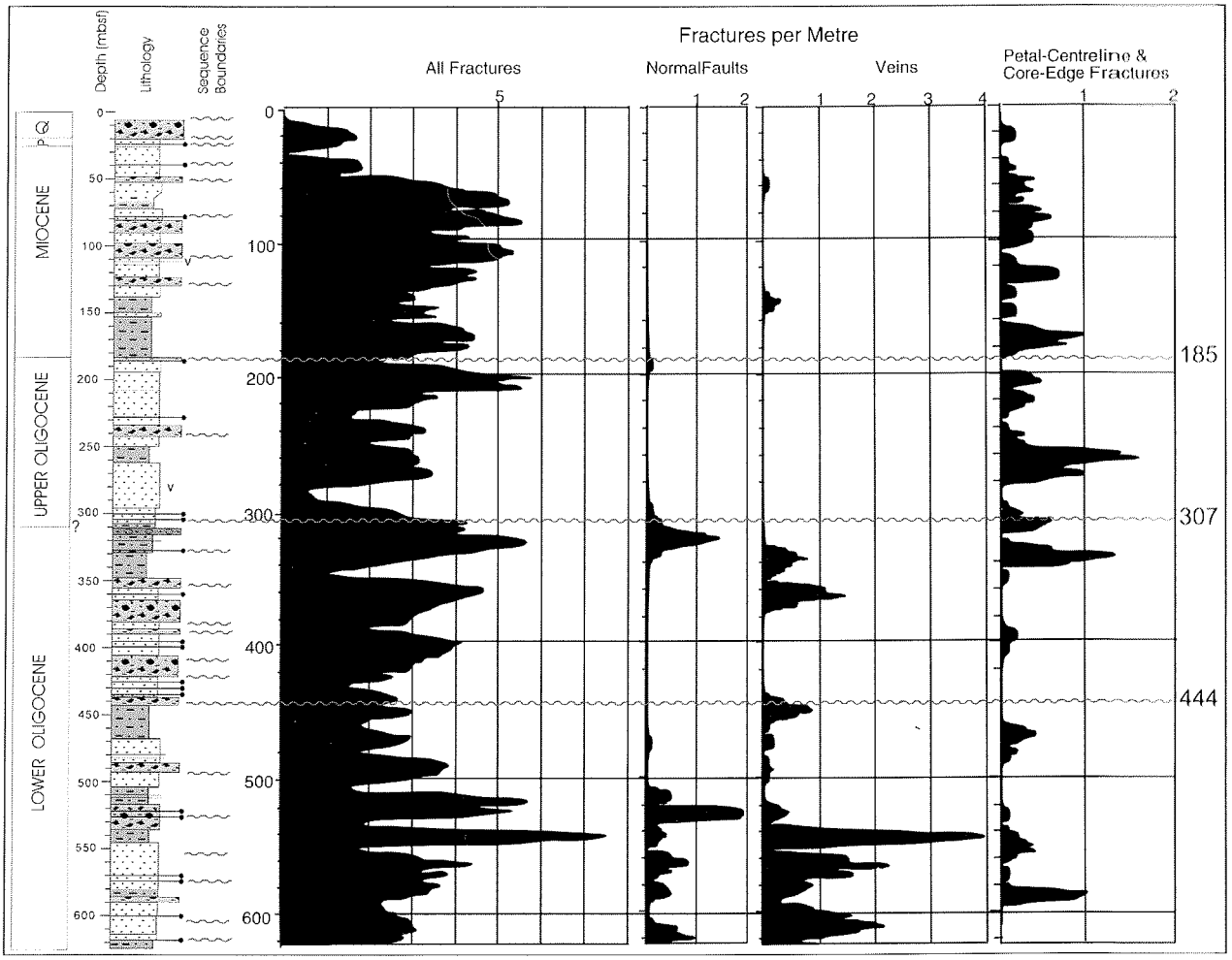

Fig. 10 - Downcore fracture densities in CRP-2A core, compared with age, depth, lithology and sequence boundaries. Histograms of fractures per metre smoothed with a 10-metre moving average window.

or drilling fluid pressures at the base of the borehole, resulting in the induced tensile fracturing.

In the upper 300 m of core, there is a correlation between many of the peaks in the density of all fractures in the core and the position of sequence stratigraphic boundaries, though there is not a one-to-one correspondence between them. Many of the sequence boundaries occur at the base of diamictites that may serve as markers for episodes of ice grounding at the drill site location. It is thus possible that the highly fractured intervals may reflect some glaciotectonic deformation. This suggestion can be tested by more detailed correlation between fracture orientation, fracture density, and independent evidence for glaciotectonic deformation (Passchier, this volume; van der Meer, this volume) in future work.

There is a high density of faults and sediment-filled veins beneath the major unconformity at 307 mbsf. There is also a peak in vein density beneath the unconformity at 444 mbsf, although much higher fault and vein densities occur deeper in the Lower Oligocene strata. Other than changes in density across the major unconformities, there appears to be no correlation between the density of the fault and vein groups and the sequence stratigraphic boundaries in the core.

INTERPRETATION OF CRP-2A FRACTURE PATTERNS

Timing of Brittle Deformation

The age of the natural fracture sets is constrained to be younger than the strata they cut. The CRP2/2A strata range in age from Early Oligocene (*c.* 30-31 Ma) to Quaternary, and natural fractures were observed in Lower Miocene and older strata. Core that has been orientated up to this point is almost all from the Oligocene section of CRP-2A core. The orientated core does not provide a continuous depth section (*i.e.*, orientated segments come from scattered portions of the Oligocene section), thus a high-resolution analysis of changes in fracture orientation and, therefore, in possible age differences of the fracture sets, is not currently possible. Given the likely errors associated with the core orientation methods, the present data are consistent with the presence of the same natural fracture sets throughout the Lower Oligocene section, and possibly also in Upper Oligocene and Lower Miocene strata. If so, this may indicate that all the faults and veins postdate the entire CRP-2 section, and thus are younger than *c.* 21 Ma, the youngest strata cut by the fracture sets.

In most cases observed in CRP-2A core, discrete

slickensided fault surfaces, microfaults and veins following fault surfaces, all crosscut pre-lithification folding and other convolute structures. This suggests faulting post-dates the ductile soft-sediment deformation interpreted to result from downslope mass movement and/or glaciotectonic deformation (Passchier, this volume). There is evidence that clastic sediment was injected along pre-existing normal-displacement microfaults. This indicates that at least some of the faulting predates complete lithification of the strata. Because the sediment-filled and cataclastic faults have the same orientations, this pre-lithification faulting appears to have been controlled by the same stresses that caused later, brittle faulting. Thus, rather than a discrete faulting episode of Miocene age, faulting likely began in the Oligocene, concomitant with later stages of deposition of the sedimentary section. Ongoing rift-related faulting controlled by a similar stress field continued through Oligo-Miocene times. The mode of faulting appears to have changed from microfaulting associated with sediment injection in incompletely dewatered rocks, to brittle faulting forming microfaults and slickensided fault surfaces. Cementation by carbonate material and precipitation of calcite and sulfides along fault surfaces appears to post-date faulting, at least in the lower portions of CRP-2A core. It is important to determine when these diagenetic changes occurred in the lithification history of the CRP-2A strata, as it will provide a relative age indicator for the microfaulting.

Stress History from Natural Fracture Sets

The conjugate geometry and normal-sense displacement associated with all the microfaults documents a vertical maximum principal stress. Because conjugate arrays cut the entire CRP-2A section, this normal-faulting stress regime must have been in place during the formation of all faults in these strata. Because we have no constraint on the relative timing of the north-northeast and east-west striking conjugate fault arrays, we can not determine whether these represent discrete deformation episodes or if their formation overlapped in time. One possibility is that development overlapped in time, with the orientation of the two horizontal stresses remaining approximately constant, but the relative magnitudes switching (*cf.* Angelier et al., 1984). Permutation between a north-northeast and a west-northwest trending maximum horizontal stress could result from far-field stress changes or from the more local effect of stress release following formation of one fracture trend, causing the perpendicular direction to become the maximum horizontal stress. A second alternative for forming coeval fault sets at high angles to each other is a triaxial strain regime in which extension occurs in both northeast and southwest directions simultaneously (*e.g.*, Reches, 1978; Krantz, 1988), however this strain regime is unlikely to form subperpendicular sets such as we observe in CRP-2A.

Contemporary Stress Directions

Robust constraints can be placed on the *in situ* contemporary stress regime in the vicinity of the CRP-2A drillsite. The presence of induced disc fractures and petal-centreline and related fractures indicates relatively high magnitude horizontal stresses are present. The strong preferred orientation of the petal-centreline group indicates strongly anisotropic horizontal stresses and documents a N10W-trending maximum horizontal stress. Because this trend is at 20° to the slope trend on the seafloor where the drillsite is located, it does not appear to be significantly influenced by local topographic stresses. Modeling studies by Li and Schmitt (1998) indicate that the presence of both disc and petal-centreline fractures is compatible with either a normal faulting or strike-slip faulting stress regime, in the sense of Anderson (1951), whereas the occurrence of discs alone would require a thrust-faulting regime. The analysis of the contemporary stress regime presented by Moos et al. (this volume), based on the presence of tensile induced fractures, the absence of borehole breakouts, and frictional constraints, also indicates either a normal faulting or strike-slip faulting stress regime.

The contemporary stress orientations are not compatible with the interpretations for the stress regime present during formation of the natural fracture sets. In a normal faulting regime, the N10W-S10E oriented contemporary maximum horizontal stress would induce conjugate arrays of N10W-striking normal faults. The natural fracture arrays in the Oligocene strata consist of north-northeast and ~east-west striking conjugate normal fault arrays.

Regional Implications

There is a striking similarity between the average fault orientations we have documented in the Oligocene strata cored in CRP-2A and both seismically-mapped offshore regional faults in the Cape Roberts region (Hamilton et al., 1998) and mesoscale faults mapped in outcrops onshore in the Transantarctic Mountains (Wilson, 1995). Wilson (1995) documented north-northeast-striking normal faults along the Transantarctic Mountains Front and, based on the fission track interpretations of Fitzgerald (1992), inferred they were post-55 Ma in age. East-northeast striking normal faults, developed primarily in proximity to transverse structures segmenting the rift flank, were also inferred to be Cenozoic in age, but no tighter age constraints were possible. The parallelism between the syn- to post-Oligocene faults in the CRP-2A strata and the faults cutting bedrock along the onshore portion of the Transantarctic Mountains Front indicates that development of all of these faults may be Oligocene or younger in age. This postulate can be tested during CRP-3 drilling, by comparing fault patterns in older strata with those documented here in Oligocene strata. As found onshore, there are no natural fracture sets in the sedimentary strata that parallel the overall north-northwest trend of the Transantarctic Mountains Front. Wilson (1995) interpreted this pattern to reflect oblique rifting along the rift boundary during the Cenozoic. It is intriguing that the contemporary stress orientations *are* oriented as expected for contemporary east-northeast extension across the Transantarctic Mountains Front.

ACKNOWLEDGEMENTS

This work was funded by NSF grant OPP-9527394 to T.J. Wilson. We thank the drilling crew for the creation of the abundant drilling-induced fractures in CRP-2A core. Successful execution of our core fracture logging depended on the careful work of the CRP-2 core processors, Jo Anderson, Ed Butler, Nick Jackson and Sonya Bryce. Eric Plankell carried out core scanning and helped us to compile and plot the fracture data. Orientation of the core would not have been possible without the orientated downhole logs acquired by Christian Buecker, Jason Brink, Erich Scholz and Thomas Wonik, and the analysis of BHTV data by Dan Moos, of dipmeter data by Rich Jarrard, and of paleomagnetic data by Gary Wilson. DMT, Germany, provided reduced rates for lease of the CoreScan® for the Cape Roberts Project and Nodi Rafat donated his time to help with setup of the instrument at the Drill Site Laboratory. We thank Rick Allmendinger and Neil Mancktelow for providing stereonet programs used for our data analysis. Francesco Salvini and Andrew Evans provided very helpful reviews that improved both the clarity of the paper and the interpretations we present (though they may not agree with all of the latter).

REFERENCES

Anderson E.M., 1951. *The Dynamics of Faulting*. Oliver & Boyd, Edinburgh, 206 p.

Angelier J., Colletta B. & Anderson R.E., 1984. Neogene paleostress changes in the Basin and Range: A case study at Hoover Dam, Nevada-Arizona. *Geological Society of America Bulletin*, **96**, 347-361.

Bankwitz P. & Bankwitz E, 1995. Fractographic features on joints of KTB drill cores (Bavaria, Germany). In: Ameen M.S. (ed.), *Fractography: Fracture Topography as a Tool in Fracture Mechanics and Stress Analysis, Geol. Soc. Spec. Publ.*, **92**, 39-58.

Barrett P.J., Henrys S., Bartek L.R., Brancolini G., Busetti M., Davey F.J., Hannah M.J. & Pyne A.R., 1995. Geology of the margin of the Victoria Land basin off Cape Roberts, southwest Ross Sea. In: Cooper A.K., Barker P.F. & Brancolini G. (eds.), *Geology and Seismic Stratigraphy of the Antarctic Margin, Antarctic Research Series*, **68** AGU, Washington, 183-208.

Bell J.S., 1996. In situ stresses in sedimentary rocks (Part I): Measurement techniques. *Geoscience Canada*, **23**, 85-100.

Busetti M., 1994. A new constraint for the age of unconformity U6 I the Ross Sea. *Terra Antartica*, **1**, 523-526.

Cape Roberts Science Team, 1998. Initial Report on CRP-1, Cape Roberts Project, Antarctica. *Terra Antartica*, **5**(1), 187 p.

Cape Roberts Science Team, 1999. Initial Report on CRP2/2A, Cape Roberts Project, Ross Sea, Antarctica. *Terra Antartica*, **6**(1/2), 173p.

Cooper A.K., Davey F.J. And Behrendt J.C., 1987. Seismic stratigraphy and structure of the Victoria Land Basin, western Ross Sea, Antarctica. In: A.K. Cooper and F.J. Davey (Editors), *The Antarctic Continental Margin: Geology and Geophysics of the Western Ross Sea*. (Circum-Pacific Counc. Energy and Mineral Resour. Earth Sci. Ser., 5B) Houston, TX, 27-65.

Del Ben, A., Finetti, I., Pipan, M., Sauli, C., and Ping, Fu, 1993. Seismic Study of the Structure, Stratigraphy and Evolution of the Ross Sea (Antarctica). In: I. Finetti and C. Roda (Editors), *Bollettino di Geofisica Teorica ed Applicata*, **XXV, 137-138**, 9-106.

Engelder T., 1987. Joints and shear fractures in rock. In: Atkinson B. (ed.), *Fracture mechanics of Rock*, Academic Press, London, 27-69.

Fitzgerald P.G., 1992. The Transantarctic Mountains of southern Victoria Land: The application of apatite fission track analysis to a rift shoulder uplift. *Tectonics*, **11**, 634-662.

Hamilton R.J., Sorlien C.C., Luyendyk B.P., Bartek L.R. & Henrys S.A., 1998. Tectonic regimes and structural trends off Cape Roberts, Antarctica. *Terra Antartica*, **5**(3), 261-272.

Iverson, N.R., Hoover T.S. & Hooke R., 1996. A laboratory study of sediment deformation: stress heterogeneity and grain-size evolution. *Annals of Glaciology*, **22**, 167-175.

Krantz R.W., 1988. Multiple fault sets and three-dimensional strain: theory and application. *Journal of Structural Geology*, **10**, 225-237.

Kulander B.R., Dean S.L. & Ward B.J. Jr., 1990. *Fractured Core Analysis: Interpretation, Logging, and Use of Natural and Induced Fractures in Core*. American Association of Petroleum Geologists Methods in Exploration Series, No. 8, 88 p.

Li Y. & Schmitt D.R., 1997. Well-bore bottom stress concentration and induced core fractures. *American Association of Petroleum Geologists Bulletin*, **81**, 1909-1925.

Li Y. & Schmitt D.R., 1998. Drilling-induced core fractures and in situ stress. *Journal of Geophysical Research*, **103**, 5225-5239.

Lorenz J.C., Finley S.J. & Warpinski N.R., 1990. Significance of coring-induced fractures in Mesaverde core, northwestern Colorado. *American Association of Petroleum Geologists Bulletin*, **74**, 1017-1029.

Maltman A.J., 1987. Shear zones in argillaceous sediments – an experimental study. In: Jones, M.E. & Preston R.M.F. (eds.), *Deformation of Sediments and Sedimentary Rocks, Geological Society Special Publication*, **29**, 77-87.

Maltman A.J., 1988. The importance of shear zones in naturally deformed wet sediments. *Tectonophysics*, **145**, 163-175.

Obert L. & Stephenson D.E., 1965. Stress conditions under which core disking occurs. *Society of Mining Engineers Transactions*, **232**, 227-235.

Plumb R.A. & Cox J., 1987. Stress directions in eastern North America determined to 4.5 km from borehole elongation measurements. *Journal of Geophysical Research*, **92**, 4805-4816.

Ramsay J.R., 1980. The crack-seal mechanism of rock deformation. *Nature*, **284**, 135-139.

Reches Z., 1978. Analysis of faulting in three-dimensional strain field. *Tectonophysics*, **47**, 109-129.

Salvini F., Brancolini G., Busetti M., Storti F., Mazzarini F., and Coren F., 1997. Cenozoic geodynamics of the Ross Sea region, Antarctica: Crustal extension, intraplate strike-slip faulting, and tectonic inheritance. *J. Geophys. Res.*, **102**, 24,669-24,696.

Suppe, J., 1985. *Principles of Structural Geology*. Prentice Hall, Englewood, New Jersey, 537 pp.

Wilson T.J., 1992. Mesozoic and Cenozoic kinematic evolution of the Transantarctic Mountains. In: Yoshida Y., Kaminuma K. & Shiraishi K. (eds.), *Recent Progress in Antarctic Earth Science*, Terra Sci., Tokyo, 303-314.

Wilson T.J., 1995. Cenozoic transtension along the Transantarctic Mountains-West Antarctic rift boundary, southern Victoria Land, Antarctica. *Tectonics*, **14**, 531-545.